#### Research Article

Garima Mittal, Sang Woo Lee, and Kyong Y. Rhee\*

# Reduced graphene oxide coating on basalt fabric using electrophoretic deposition and its role in the mechanical and tribological performance of epoxy/basalt fiber composites

https://doi.org/10.1515/ntrev-2021-0091 received August 2, 2021; accepted September 7, 2021

Abstract: The interfacial bonding between the fiber and matrix plays a pivotal role in deciding the mechanical performance of fiber-reinforced composites. Basalt fibers, due to the absence of surface functional groups, do not interact potentially with the matrix and hence it leads to insufficient load-carrying capacity of the composite. Incorporating nanomaterials in the matrix and surface treatment of the reinforced fiber can improve the fibermatrix interface. However, poor dispersion of nanomaterials and the complexity of surface treatment methods restrict their industrial applications. Coating nanomaterials directly onto the fiber surface has the potential to distribute the nanomaterials uniformly, along with strengthening the interfacial bonding between the fiber and matrix. In this study, graphene oxide was coated on the basalt fabric through electrophoretic deposition (EPD), and was further reinforced into the epoxy matrix. The aim of this study is to examine the effects of graphene oxide-coated basalt fiber using EPD on the mechanical and tribological performance of the composite. For comparison, epoxy/basalt composites and graphene oxide-coated epoxy/basalt composites were also prepared. Results showed that due to the improved fiber-matrix bonding and uniform distribution of graphene oxide, the coated basalt-reinforced composites showed better tensile strength and less wear loss.

**Keywords:** fiber-reinforced polymer, tensile strength, coefficient of friction, wear, basalt fiber

Garima Mittal, Sang Woo Lee: Department of Mechanical Engineering (BK21 Four), College of Engineering, Kyung Hee University, Yongin 446-701, Republic of Korea

# 1 Introduction

Fiber-reinforced composites have revolutionized the automobiles, aerospace, and construction industries by replacing many metal parts because of their superior strength-toweight ratio [1,2]. The high mechanical performance of a fiber-reinforced composite is significantly influenced by its interfacial bond strength between the fiber and the reinforced matrix, and hence, for an efficient load transfer from matrix to the fiber, a strong interfacial bonding is a prerequisite [3,4]. A low interfacial adhesion due to the stress concentration at the interface could lead to crack propagation, leading to severe damage and in-plane strength reduction [5]. Untreated fibers usually possess a smooth surface that is not suitable for anchoring the matrix onto it [6]. Additional nano- or micro-scale particles are used as a secondary reinforcement to fill this interfacial gap between filler and the matrix. These composites are sometimes referred to as multi-scale composites. Using nanomaterials can improve the performance of the multi-scale composites, such as improved toughness and stiffness and better friction and wear resistance [7,8]. Besides, nanomaterials possessing distinct properties than their bulk counterparts provide an opportunity to develop composites with the desired properties and functionality [9]. Nanomaterials, due to their high surface-to-volume ratio, are used in small quantities. So, there is no weight penalty. To this end, nanomaterials are usually dispersed into the matrix, which helps to fill the voids in the matrix [10,11]. However, at the same time, nanomaterials, due to van der Waal interactions, form agglomerates, hindering their uniform dispersion into the matrix, which sometimes leads to void formation and poor fibermatrix interactions. Hence, the surface of reinforcing nanomaterials is usually treated with a coupling agent that helps in the uniform dispersion of nanomaterials as well as in improving the mechanical and tribological performance of the reinforced composite [12–14]. Sizing or surface treatment

<sup>\*</sup> Corresponding author: Kyong Y. Rhee, Department of Mechanical Engineering (BK21 Four), College of Engineering, Kyung Hee University, Yongin 446-701, Republic of Korea, e-mail: rheeky@khu.ac.kr

of the fiber surface are other ways to improve the fiber–matrix interfacial bonding strength [15]. During sizing, the fiber surface is coated with a protective material that protects the fiber surface against friction and wear during production and introduces some surface features that help attach the matrix with the fiber [16]. In surface treatment, chemical or physical methods are used to modify the fiber surface that sometimes deteriorate the fiber structure as well as its performance [17,18]. Among all, attaching/grafting nanomaterials onto the fiber surface seems the best way to potentially improve the overall properties of multi-scale composites, because it offers a uniform distribution of the nanomaterial throughout the matrix along with improving the bonding of the fibers with the matrix.

Recently, with industries preferring eco-friendly and cost-efficient production materials, basalt fiber, a natural fiber produced from solidified volcanic lava (basalt rock), can be a suitable alternative to the expensive carbon fiber, possessing better Young's modulus (100–110 GPa) and tensile failure (4.15-4.840 GPa) than E-type glass fiber [19]. As a result of its exceptional environmental stability and high mechanical strength, it is used in numerous industrial applications. The absence of surface functional groups at the basalt fiber surface limits its interfacial interaction with the matrix. Therefore, nanomaterial was directly coated on the fiber surface in this study rather than dispersing it into the matrix. Coating methods such as chemical vapor deposition, spray coating, hydrothermal coating, and dip coating are commonly used [20,21]. However, either the non-uniform deposition and poor adhesion or complexity and high-production cost make them unsuitable for large-scale applications. Electrophoretic deposition (EPD), a widely used industrial coating method that is very simple, time and cost effective, and environmentally friendly, is used to coat uniform and well-adhered coatings [22]. In EPD, charged particles suspended into the medium travel toward oppositely charged electrodes depending on their charge due to the application of an electric field. EPD provides the freedom to control the coating thickness by altering the deposition time, mass, and concentration of the suspended material and applied voltage. There are other advantages like deposition at room temperature, no adverse effect on the coating material or the substrate, and deposition of a wide range of conductive materials on various surfaces.

In this study, graphene oxide (GO) is coated on basalt fabric (BF) without any chemical groups or coupling agents to improve its interaction with the epoxy matrix. Along with its unique mechanical, thermal, electrical properties, and good chemical stability, the layered structure of GO or reduced GO (rGO) helps in providing a better coating by

covering the fiber surface parallelly [23,24]. This study focuses on the uniform distribution of rGO throughout the composite and enhancement of the interfacial bonding between basalt fiber and epoxy. Not many reports are available on the deposition of rGO on basalt fiber using EPD to the best of our knowledge, even though plenty of reports are available for carbon fibers as a substrate. To understand the effects of rGO coated basalt fiber on its mechanical and tribological properties, tensile and wear tests were conducted and compared with GO-reinforced epoxy/basalt fiber and pure epoxy/basalt fiber composites.

# 2 Experimental

## 2.1 Materials

Basalt fiber (plain-woven type fabric) was obtained from Seotech company, South Korea. Reagent grade hydrazine hydrate ( $N_2H_4$  50–60%), graphite (flakes, 99% carbon basis), and potassium permanganate (ACS reagent,  $\geq 99.0\%$ ) were purchased from Sigma Aldrich, Republic of Korea. Hydrogen peroxide (30%), sulfuric acid (70%), acetone (>99.5%), de-ionized (DI) water, and HCl (35–37%) were purchased from Daejung Chemicals, South Korea. Epoxy resin (EPOKUKDO YD-115) and curing agent (DOMIDE G-A0533) were ordered from Kukdo Chemicals, Republic of Korea.

#### 2.2 EPD of GO on basalt fiber

GO coated on BF was prepared from graphite through modified Hummer's method [25], where graphite and potassium permanganate, in a 1:3 ratio, were slowly mixed into 70 mL of hydrochloric acid in the presence of an ice bath. After continuously mixing for 30 min at 35°C, 150 mL of DI water was slowly mixed into the solution, and because of an exothermic reaction, the solution temperature reached up to 95°C. After 15 min of stirring, again 500 mL of DI water was mixed into the solution, and as the solution temperature reduced after 5 min, 15 mL of 30% hydrogen peroxide was mixed drop-wise to stop the reaction, which turned the solution color brown to bright yellow with the generation of bubbles. The resulting mixture was filtered, followed by washing with 1% HCl solution and DI water 2-3 times (till the pH became  $\sim$ 7). The obtained powder was GO.

EPD was used to coat the GO powder on BF without any coupling agent or chemical. To that end, an aqueous

bath solution of homogeneously dispersed GO powder (1 mg/mL) was used, where GO exhibited strong hydrophilicity due to having various oxygen-containing (epoxide, hydroxyl, and carbonyl) groups, leading to the formation of a stable colloidal aqueous suspension [26,27]. BF with  $100 \,\mathrm{mm} \times 120 \,\mathrm{mm}$  dimensions was used to coat with GO, which was immersed into acetone for 24 h at 80°C for the complete removal of the sizing agent. BF is a non-conductive material made up of melted lava rocks, and EPD is only suitable for conductive substrates. Therefore, BF was attached to a copper sheet, which acted as an electrode (anode), as GO deposition is an anodic reaction due to the negative charge on the GO sheet. For our EPD set-up, two copper plates (99.96% purity; 0.2 mm thickness), acting as positive and negative electrodes, were immersed in a 2L aqueous suspension of GO, which was stirred constantly using a magnetic stirrer during deposition. The distance between the electrodes was around 2 cm, and a DC bench power supply (RS Pro IPS-303DD, China) was used. The EPD was performed at 5 V for 10 min. After EPD, the loosely attached GO flakes were removed by dipping the coated fabric into DI water twice, followed by drying at 50°C for 12 h. The coated material was referred to as GOcoated basalt fiber (GO@Basalt).

Hydrazine hydrate is a strong reducing agent that reduced GO flakes into rGO, that is, graphene flakes [28]. To reduce GO into rGO, the GO@Basalt was treated thermo-chemically at 100°C for 24 h in the presence of hydrazine hydrate ( $\sim$ 2–3 mL). The coated material is referred as rGO-coated BF (rGO@Basalt).

# 2.3 Preparation of basalt fiber-reinforced polymer (BFRP) composites

BFRP composites were prepared through vacuum-assisted resin transfer molding (VaRTM) (Figure 1), where composites were formed using a rigid mold, greased with a releasing agent, and connected to the resin inlet and vacuum outlet tubes with valves. The BF sheets were placed in the mold, and the mold was sealed after that. The epoxy resin and hardener were mixed in a ratio of 2:1 (v/v). After degassing of resin, it was injected into the mold through suction generated via applied vacuum at the other end, and after complete immersion of BF, the vacuum was removed, and the resin inlet and vacuum outlet valves were closed to maintain the vacuum inside the mold. The epoxy resin was cured by placing the mold in an oven for 2h at 80°C. rGO@Basalt sheets were used to form rGO coated BF reinforced composites, and the formed composites were referred to as rGO@Basalt/epoxy composites.

To compare the effect of rGO@Basalt/epoxy composites, their properties were compared with GO-reinforced epoxy/BF (GO + epoxy/basalt) composites and pure epoxy/ BF (basalt/epoxy) composites. The GO + epoxy/basalt composites were prepared by dispersing GO into the acetone and sonicating for 15 min, followed by mixing into the epoxy resin. The acetone was evaporated by stirring the solution at 50°C for ~1.5 h, followed by mixing the curing agent. The BFRPs were prepared through VaRTM, and instead of rGO@Basalt, uncoated BF sheets were used for GO + epoxy/basalt composite. For basalt/epoxy composites, pure resin (no GO dispersion) and uncoated BF were used.

#### 2.4 Characterization

Field emission scanning electron microscopy (FE-SEM) (LEO SUPRA 55, GENESIS 2000) was conducted to examine the morphology of BF before and after rGO grafting. For analysis, platinum sputtering was done on the samples to enhance image quality. Raman spectroscopy (RFS 100/S; Bruker,  $\lambda = 532 \, \text{nm}$ ) was done to confirm the attachment of GO and rGO on the basalt fiber. A tensile test was conducted using a universal testing machine (Instron8871; Instron Engineering Corp., United States) to investigate the effect of rGO grafting on the BF surface and its effects on BFRP. The tensile specimens were prepared according to ASTM D638 (Figure 2). The tests were conducted at room temperature at a speed of 0.5 mm/min with six replicates for each case. Further, the fractured surface of the tensile specimen was analyzed using FE-SEM analysis.

The tribological properties of the rGO-coated BFRPs were analyzed through the ball-on-disk method using a wear test machine (Multipurpose device friction and wear tester, Neo-plus Inc., South Korea), where a SUS 314 friction ball with 12.7 mm diameter was used, and the test specimens were prepared according to ASTM D99 (30 mm × 30 mm). The test conditions were a constant load of 10 kgf at room temperature, track radius of 11.5 mm, rotation speed of 0.036 m/s, and a total distance of 325 m. For reproducibility of the results, three specimens were prepared for each case. A detailed analysis of the wear track depth (wear area) was done through a surface profilometer (Veeco Instruments Inc., United States), where the analysis was done for 100 s with 1 mg force at 0.167 µm/ sample resolutions within a measurement range of 524 µm. For reproducibility, four random points were measured for each case. Further, an FE-SEM image analysis was conducted to analyze the wear tracks of the specimens.

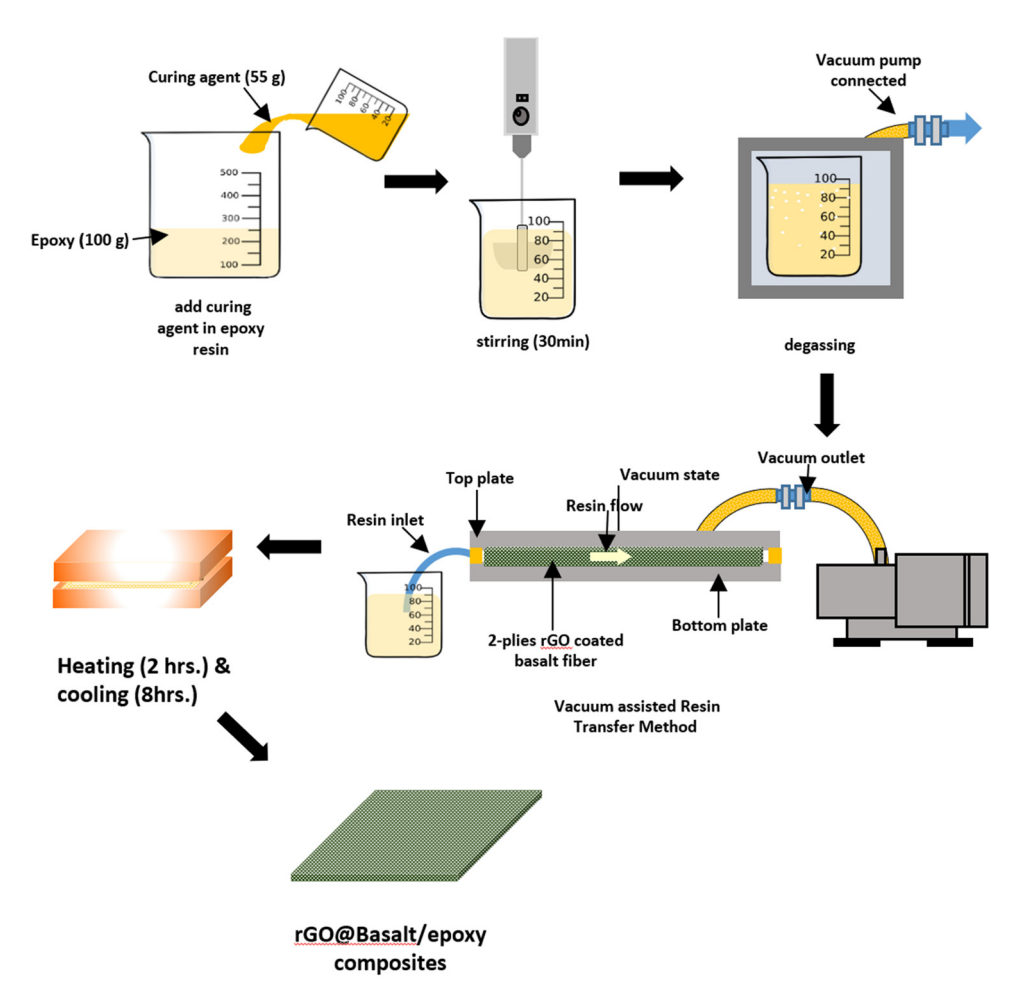


Figure 1: Schematic of the fabrication of rGO@Basalt/epoxy composites using the VaRTM method.

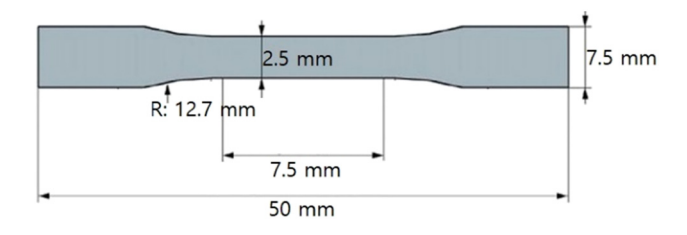


Figure 2: Specification of ASTM D638 tensile specimen.

## 3 Results and discussion

The morphological analysis of the BF before and after the EPD of GO was done using FE-SEM. Figure 3(a) represents the SEM image of an uncoated basalt fiber while Figure 3(b and d) and (c and e) shows the SEM images of BF coated with GO and rGO using EPD, respectively. The surface of uncoated BF was found smooth and clear compared to the coated BF, along with some traces of residual sizing material on the surface. The BF surface became rougher and wrinkled after the EPD of GO and rGO flakes. This happened because when the electric force was applied during EPD, GO flakes, which are negatively charged, started immigrating toward the positively charged electrode, where the BF was attached to it [29,30]. The thermal treatment at 50°C for 24 h of GO-coated BF helped it to well adhere to the GO flakes on the fabric. For rGO@Basalt, the thermochemical treatment reduced the coated GO flakes into rGO and turned the multi-layered arrangement of GO sheets (red arrows in Figure 3(b)) into a few-layered transparent graphene flakes (red arrows in Figure 3(c) and (e). These coated GO and rGO flakes on BF are very important for establishing and improving the interfacial connections throughout the composite structures with adjacent fibers and the reinforced matrix.

Figure 3(f) and (g) represent the energy-dispersive X-ray spectroscopy data of BF before and after electrodeposition of GO. Elemental peaks such as Na, Mg, Al, Ti, Fe, O, and Si were commonly found due to the elemental (alumino-silicate) composition of the basalt fiber. After

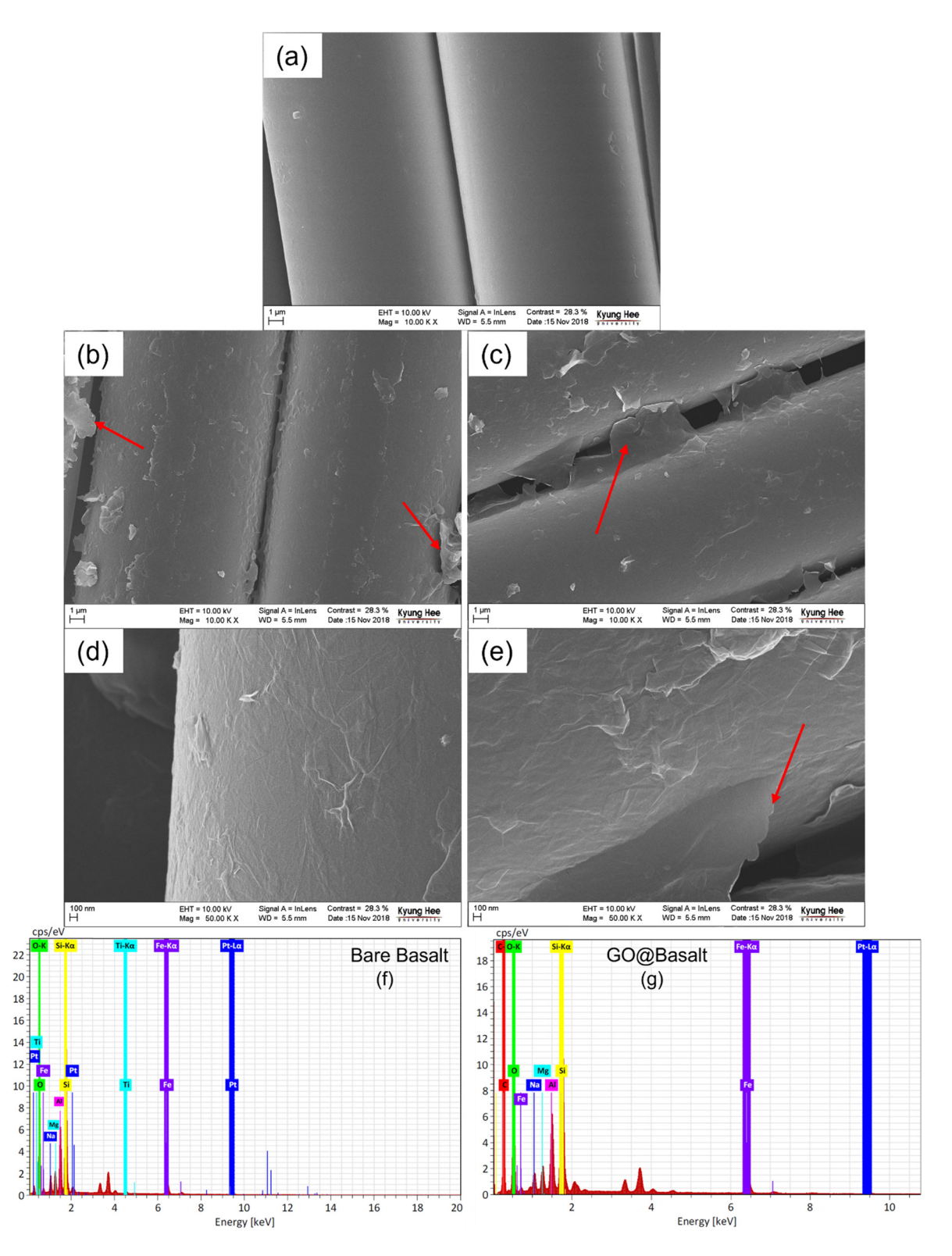


Figure 3: FE-SEM images of (a) uncoated basalt fiber, (b and c) GO@Basalt and (d and e) rGO-coated basalt fiber (rGO@Basalt). EDS spectra of uncoated basalt fiber (f) and GO@Basalt (g).

deposition of the GO, an additional carbon peak was also observed, validating the deposition of GO films.

Raman spectroscopy was done to confirm the attachment of GO and its reduction into rGO. A comparison of

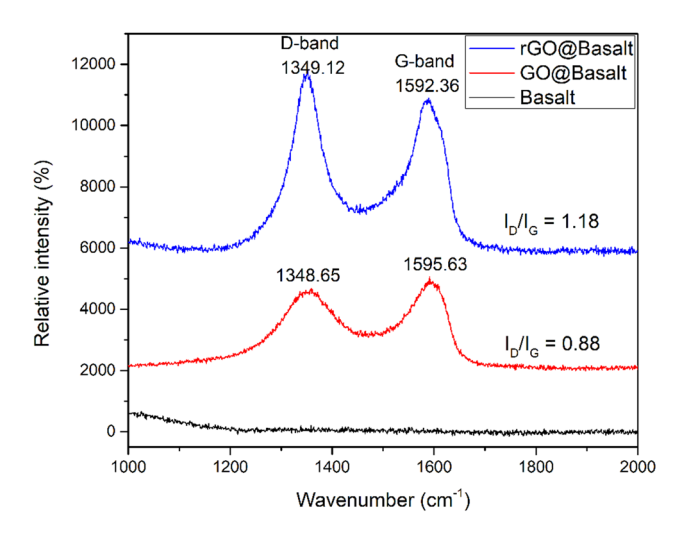


Figure 4: Raman analysis of basalt fiber (Basalt), GO-coated basalt fiber (GO@Basalt), and rGO-coated basalt fiber (rGO@Basalt).

the Raman spectra of basalt fiber before and after deposition of GO is done in Figure 4, where characteristic graphitic peaks were found after coating, which were absent in the uncoated basalt fiber. The peak that appeared at ~1,350/cm, also referred to as D-band, was because of the defects present in the graphitic ring, while the crystallinity of the graphitic ring was evident through the peak at ~1,580/cm, also referred to as G-band. The intensity of the D-band increased compared to the G-band after reduction of the GO due to the defects generated during the thermochemical reduction. The defects occurred due to the removal of oxygen-containing groups that led to the ring-opening of epoxide groups. The intensity ratio of defects and graphitic rings  $(I_D/I_G)$  is used to quantify the chemical and structural variations during reduction. The higher value of  $I_D/I_G$  indicates more defects and *vice-versa*. The  $I_D/I_G$  of rGO@Basalt was higher (1.18) than GO@Basalt, indicating the defects generated during the thermochemical reduction of GO [31].

Tensile tests were conducted to study the effect of BF electrophoretically coated with rGO on the mechanical behavior of BF-reinforced epoxy composites, and it was compared with pure BF/epoxy composites and GO-reinforced epoxy/basalt composites. Although all composites exhibited a linear mode of failure without any sign of plastic deformation, leading to a sudden failure (Figure 5(a)), the rGO-coated BF/epoxy composite showed the maximum tensile strength among all (13.7% higher than basalt/epoxy and 5.3% higher than GO + epoxy/basalt composites). The order of tensile strength was rGO@Basalt/epoxy > GO + epoxy/basalt > basalt/epoxy (Figure 5(b)). This happened because of the homogenous distribution of rGO flakes and enhanced interfacial interactions between the BF

and epoxy matrix. When an external load is applied to the specimen, it is supposed to be transferred from epoxy to BF [32]. In the absence of nanomaterials that act as an interfacial bridge, transferring the load from matrix to fiber, the crack propagates. In the case of rGO@Basalt/epoxy, homogeneously distributed rGO flakes at the fiber-matrix interface filled the interfacial gaps and helped in effective load transfer from matrix to fiber, resisted the fiber pull-out, that is, more elongation at break [33]. While in the case of GO + epoxy/basalt composites, the GO flakes helped to fill the micro- or nano-scale voids in the polymer matrix and to inhibit crack propagation and energy dissipation by acting as an obstacle [34]. However, nanomaterials, due to van der Waal interactions, form agglomerates and restrict their homogeneous dispersion into the matrix. Hence, due to agglomeration, GO flakes could not improve the tensile property of the composite by its full potential. Due to poor load transfer and voids in the matrix, the basalt/epoxy composite showed low tensile strength [35]. A similar trend was observed for fracture toughness, where the rGO@Basalt/ epoxy showed 33.4 and 12.2% improvement in fracture toughness than basalt/epoxy and GO + epoxy/basalt composites, respectively (Figure 5(d)). The tensile test data are summarized in Table 1.

Further analysis of the morphology of the fractured surface was done using SEM. Figure 6((a and b), (c and d), and (e and f)) represent the SEM images of basalt/epoxy, GO + epoxy/basalt, and rGO@Basalt/epoxy composites, respectively. It was found that the basalt fibers at the fractured surface of basalt/epoxy and GO + epoxy/basalt composites were comparatively smoother (no or less epoxy residue) than the rGO@Basalt/epoxy composite. This happened because, in the rGO@Basalt/epoxy composite, the coating of rGO fills the interfacial gap between fiber and matrix and boosts their adhesion. Hence, fibers do not pull out easily during the presence of an external force [29,33]. But the basalt/epoxy composite, due to voids and lack of reactive groups on the surface of the basalt fiber, showed insufficient load-carrying capacity and fibers came out of the matrix easily [36]. For GO + epoxy/basalt composites, even though the fiber pull-out was less compared to basalt/epoxy composites, due to inadequate dispersion of GO flakes, the bonding between the filler and matrix could not improve completely.

The tribological properties of all the composites were analyzed through friction and wear tests using the ball-on-disc method. A comparison of the friction pattern and coefficient of friction (CoF) of basalt/epoxy, GO + epoxy/basalt, and rGO@Basalt/epoxy composites are given in Figure 7(a) and (b), respectively. It was found that due

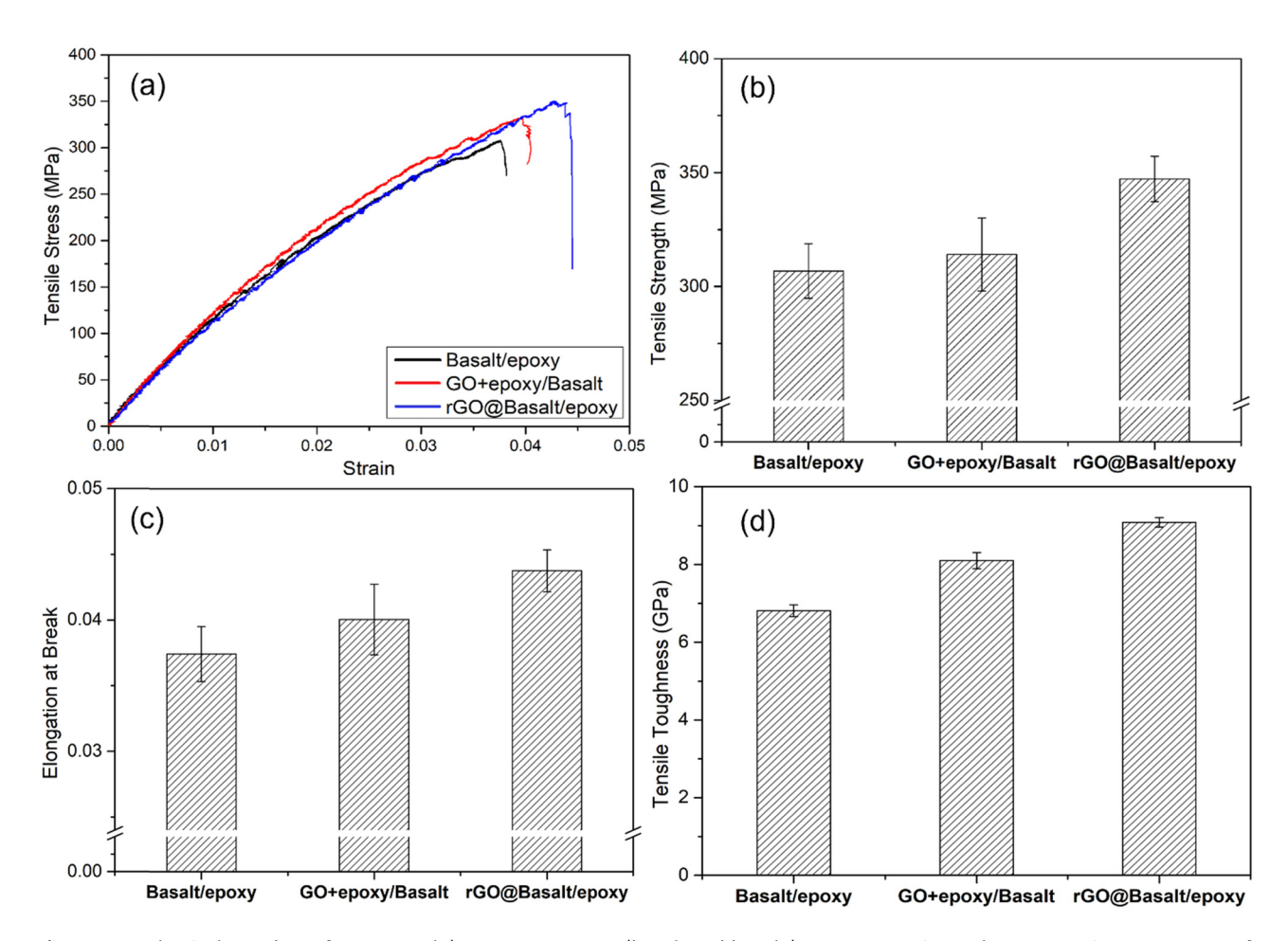


Figure 5: Mechanical test data of rGO@Basalt/epoxy, GO + epoxy/basalt and basalt/epoxy composites, where (a) strain-stress curve of tensile specimens, (b) tensile strength, (c) elongation at break, and (d) tensile toughness.

to the homogenous deposition of rGO on the basalt fiber using EPD, the friction between the zirconia ball and the rGO@Basalt/epoxy specimen decreased  $\sim$ 18% than that on basalt/epoxy and  $\sim$ 4.3% than that on GO + epoxy/basalt composites. The order of CoF was similar to the tensile strength, that is, rGO@Basalt/epoxy < GO + epoxy/basalt < basalt/epoxy. When the zirconia ball slid on the rGO@Basalt/epoxy composite specimen, the homogenously dispersed rGO flakes acted as a dry lubricant and the weakly bound layers of rGO, bonded through the van der Waals' force, started sliding [37,38]. Consequently, the friction was reduced. The CoF values are mentioned in Table 2.

The macrographs of worn samples are shown in Figure 8(a). The detailed analysis of the wear behavior of all specimens was done using a surface profilometer. The figure shows the wear test data of all the specimens, where Figure 8(b), (c), and (d) compare the wear track, wear volume, and specific wear rate of basalt/epoxy, GO + epoxy/basalt, and rGO@Basalt/epoxy composites, respectively. The cross-section view of the wear pattern shows that the wear depth and wear track width decreased after EPD of rGO on BF. The quantitative analysis of the wear data was done through the Archard equation [39],

$$V = k \cdot F \cdot S$$
,

Table 1: Summarized values of tensile strength, elongation at break, and tensile toughness of tensile specimens

Sample name	Tensile properties		
	Tensile strength (MPa)	Elongation at break	Tensile toughness (GPa)
Basalt/epoxy	306.8 (±12)	0.03742 (±0.0021)	6.8092 (±0.15)
GO + epoxy/basalt	314.1 (±16)	$0.04005 (\pm 0.0027)$	8.1013 (±0.21)
rGO@Basalt/epoxy	347.3 (±10)	0.04377 (±0.0016)	9.0859 (±0.12)

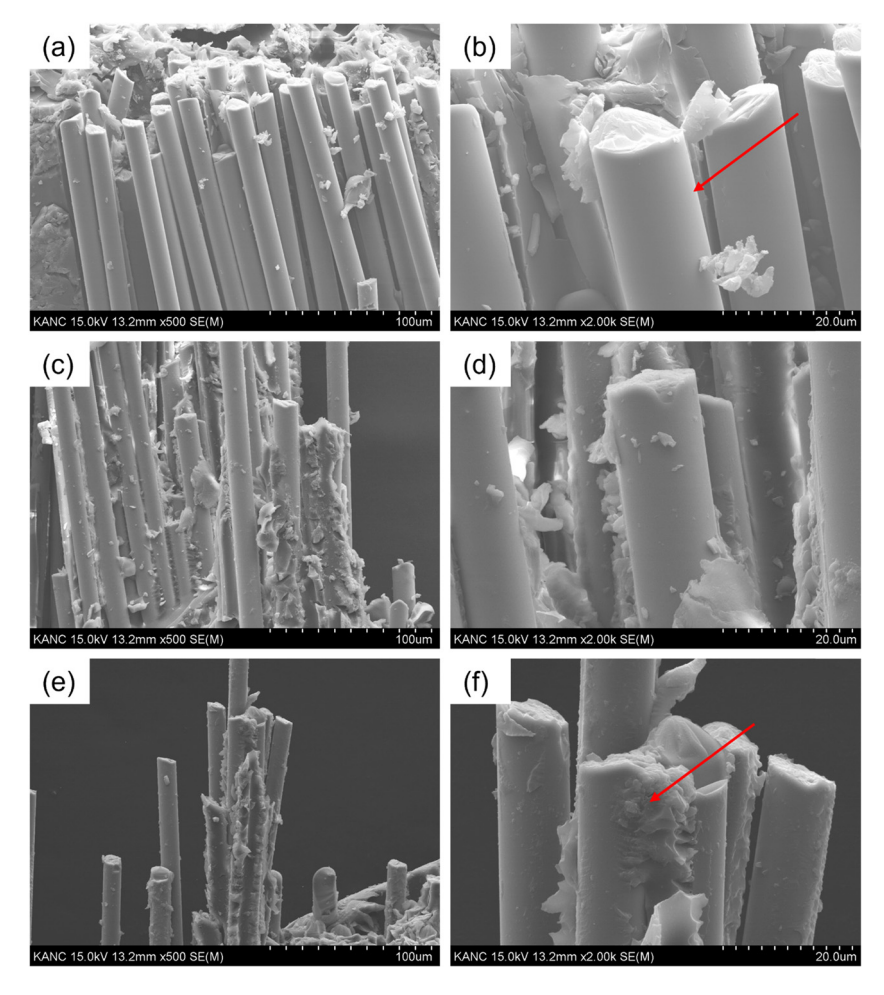


Figure 6: FE-SEM image of the fracture surface of (a and b) basalt/epoxy, (c and d) GO + epoxy/basalt, and (e and f) rGO@Basalt/epoxy composites.

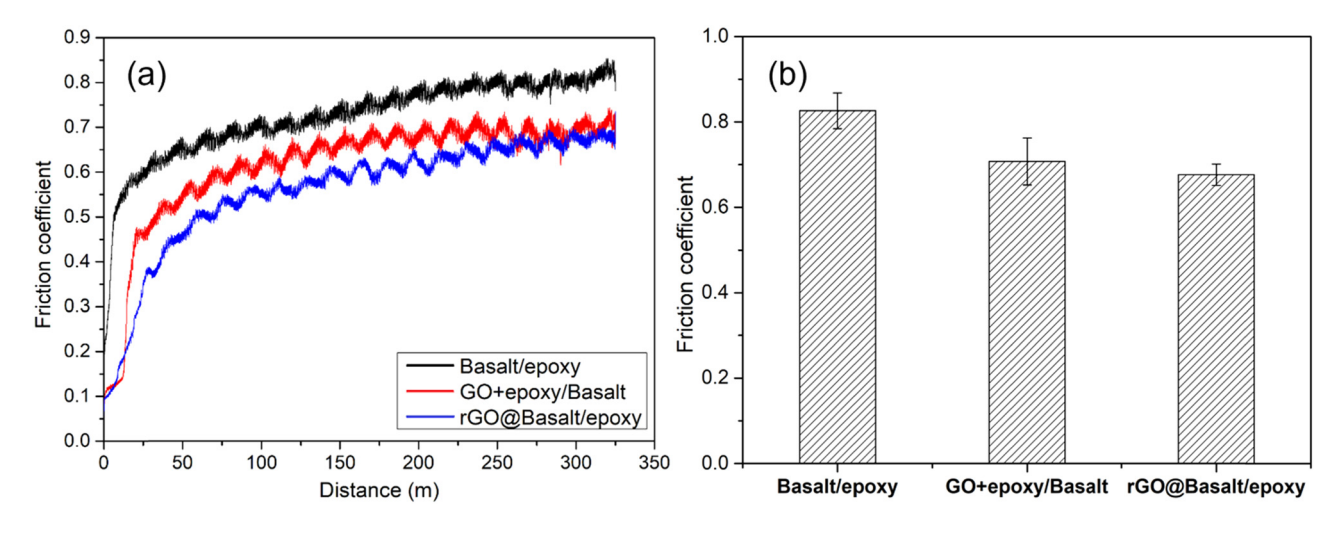


Figure 7: (a) Friction test pattern and (b) CoF of basalt/epoxy, GO + epoxy/basalt, and rGO@Basalt/epoxy composites wear specimens.

where V, k, F, and S are wear volume, wear rate, normal load, and zirconia ball's sliding distance. The value of

wear volume (*V*) was obtained through the cross-sectional area (*A*) of the wear track and wear track radius (*r*) using

Table 2: Summarized values of CoF, wear volume, and specific wear rate of basalt/epoxy, GO + epoxy/basalt, and rGO@Basalt/epoxy composites wear specimens

Sample name	Tribological properties			
	СоF	Wear volume (mm³)	Specific wear rate (mm <sup>3</sup> /N m)	
Basalt/epoxy	0.8262 (±0.0042)	16.120 (±0.54)	$0.01645~(\pm 5.1 \times 10^{-4})$	
GO + epoxy/basalt	0.7074 (±0.0055)	11.042 (±0.71)	$0.01127~(\pm 6.6 \times 10^{-4})$	
rGO@Basalt/epoxy	$0.6764~(\pm 0.0025)$	10.146 (±0.48)	$0.01035\ (\pm4.5\times10^{-4})$	

$$V = 2\pi r A$$
.

Since the wear depth and width were lower for the rGO@Basalt/epoxy specimen, the lower volume loss and lower wear loss were observed. The order of specific wear loss was in accordance with the tensile test data, that is, rGO@Basalt/epoxy < GO + epoxy/basalt < basalt/epoxy composites. The summary of the wear test data is given in Table 2. This is because of the improved interfacial bonding between the fiber and matrix after the uniform

deposition of rGO on the BF, leading to better wear resistivity of the composite [40]. Moreover, the sliding of the weakly bound rGO layers provided additional smoothness to the wear track [41]. The basalt/epoxy composite, due to the presence of voids in the absence of reinforcing material, showed the deepest wear track and highest wear loss. For the GO + epoxy/basalt specimens, even though the wear track was smooth due to the GO acting as a dry lubricant, the inhomogeneous dispersion of GO

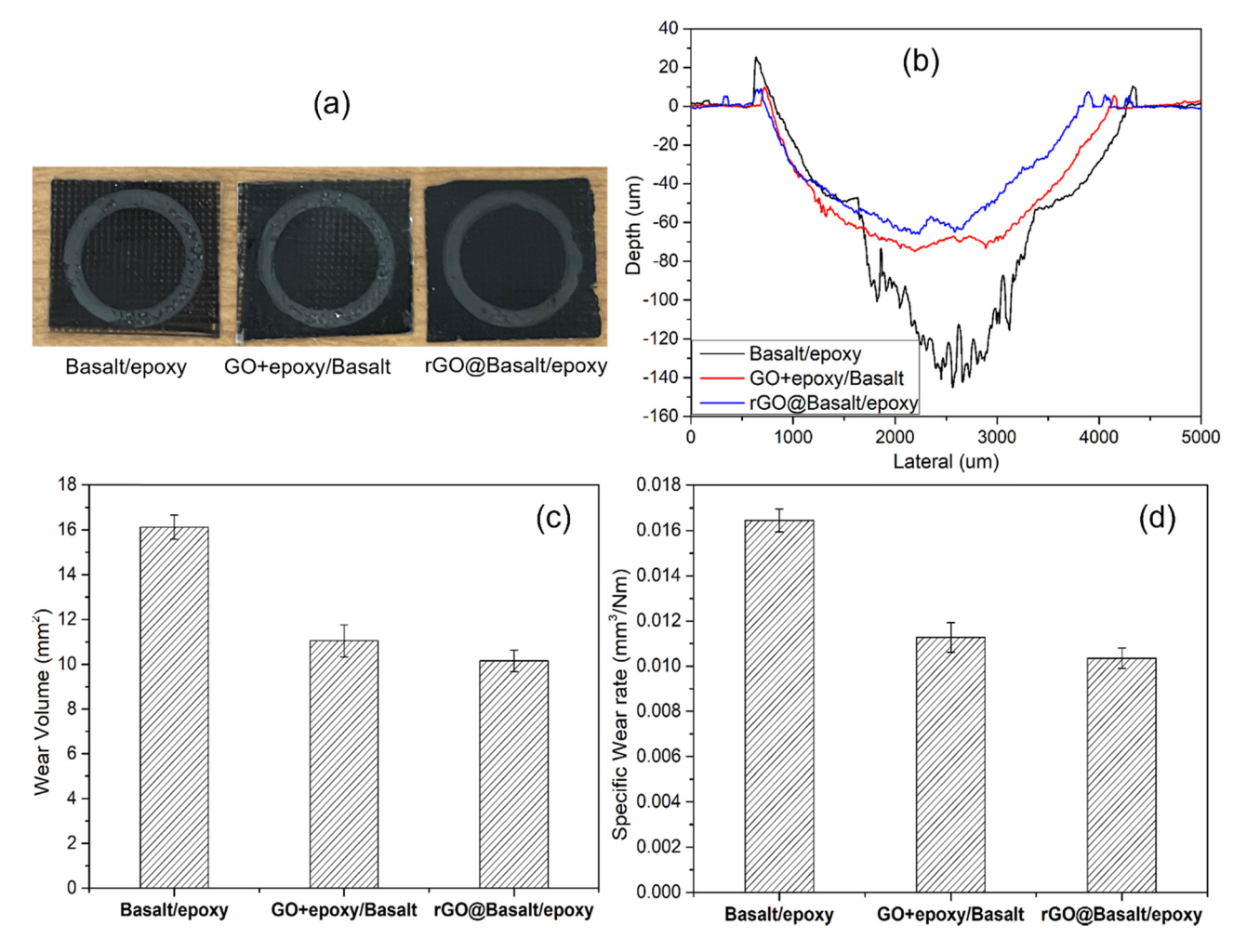


Figure 8: Comparison of (a) full wear track, (b) cross-section of wear track, (c) wear volume, and (d) specific wear rate of basalt/epoxy, GO + epoxy/basalt, and rGO@Basalt/epoxy composites wear specimens.

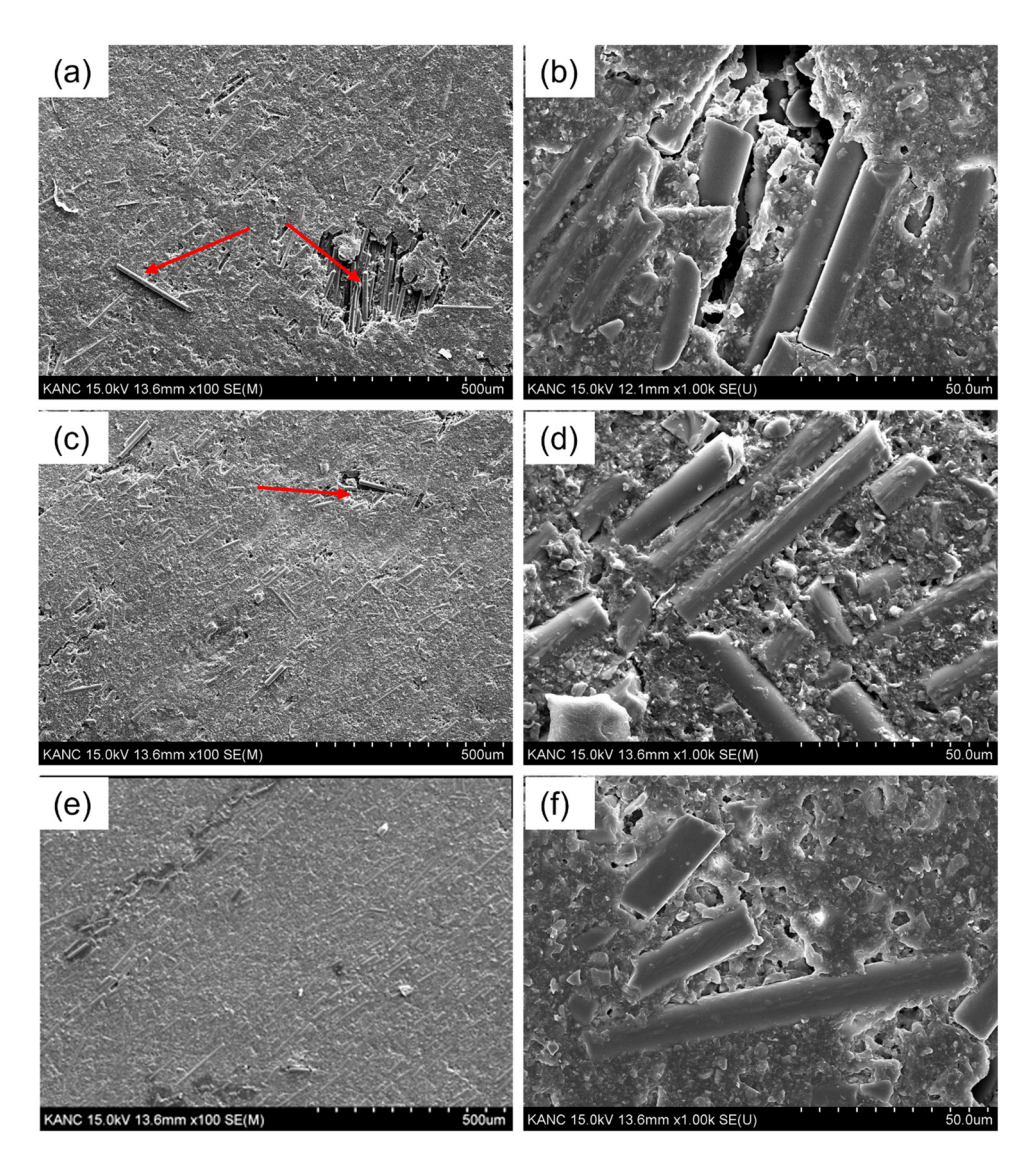


Figure 9: FE-SEM image of wear tracks of (a and b) basalt/epoxy, (c and d) GO + epoxy/basalt, and (e and f) rGO@Basalt/epoxy composites.

flakes, and the poor fiber-matrix interaction could not resist fiber pull-out during ball sliding, and hence, more wear loss. The wear data are presented in Table 2.

The morphology of the wear tracks of all specimens is examined using FE-SEM, and Figure 9((a and b), (c and d), and (e and f)) represent the FE-SEM images of basalt/epoxy, GO + epoxy/basalt, and rGO@Basalt/epoxy composites, respectively. The wear track of basalt/epoxy was rough and showed many voids along with broken fibers due to the poor matrix–fiber interactions. The GO + epoxy/basalt also showed a rough track but with less debris and fewer broken fibers due to the dry lubrication of dispersed GO flakes. The rGO@Basalt/epoxy specimen showed the smoothest wear track with fewer voids due to the improved interfacial adhesion between fiber and matrix after rGO coating that restricted the pulling-out and

breaking of basalt fiber [42]. These data were in accordance with the tensile data, proving that EPD of rGO onto BF improves interfacial interactions when compared to the random dispersion of nanomaterials into the matrix.

## 4 Conclusion

This study mainly focused on coating the nanomaterials directly on the fiber surface for their homogenous dispersion throughout the matrix and enhancing the interfacial bonding between fiber and matrix in multi-scale composites. The performance analysis of these nanomaterial coated fiber-reinforced polymer composites was compared

with the randomly distributed nanomaterial in the matrix/ fiber composites. BF was coated with GO using EPD, which was later reinforced into the epoxy matrix using the VaRTM technique. The morphological analysis through FE-SEM showed that after deposition, the fiber surface became rougher due to the attachment of GO and rGO flakes that helped in anchoring the epoxy chains onto the fiber surface. Also, the deposition of GO directly onto the fiber gave rise to a homogeneous distribution throughout the matrix. After comparing its mechanical and tribological properties with GO-reinforced epoxy/fiber and pure epoxy/ fiber composites, it was found that coated basalt fiber-reinforced composites exhibited better tensile strength, lower CoF, and lower wear loss. This can be explained due to the fact that the uniform distribution of rGO flakes throughout the matrix and improved interfacial bonding between the fiber and matrix, restricted fiber pull-out, diverted crack propagation, and limited wear track.

Funding information: This study was supported by the Basic Science Research Program through the National Research Foundation of Korea (NRF) and was funded by the Ministry of Education, Science, and Technology (Project number: 2020R1A2B5B02002203).

Author contributions: All authors have accepted responsibility for the entire content of this manuscript and approved its submission.

**Conflict of interest:** Authors state no conflict of interest.

### References

- Nasir T, Kalaf O, Asmael M, Zeeshan Q, Safaei B, Hussain G, et al. The experimental study of CFRP interlayer of dissimilar joint AA7075-T651/Ti-6Al-4V alloys by friction stir spot welding on mechanical and microstructural properties. Nanotechnol Rev. 2021:10(1):401-13.
- Guo Z, Zhu Q, Wu W, Chen Y. Research on bond-slip performance between pultruded glass fiber-reinforced polymer tube and nano-CaCO3 concrete. Nanotechnol Rev. 2020;9(1):637-49.
- DiBenedetto AT. Tailoring of interfaces in glass fiber reinforced polymer composites: a review. Mater Sci Eng A. 2001;302(1):74-82.
- Liu F, Wang D, Liu J, Wei H, Zhang H, Xu J, et al. Reviews on interfacial properties of the carbon fiber reinforced polymer composites. J Phys Conf Ser. 2020;1637:012027.
- Mittal G, Dhand V, Ryu JI, Rhee KY, Kim H-J, Jung DH. Fabrication of modified MMT/glass/vinylester multiscale

- composites and their mechanical properties. J Nanomater. 2015:2015:506029.
- Zhou A, Wei H, Liu T, Zou D, Li Y, Qin R. Interfacial technology [6] for enhancement in steel fiber reinforced cementitious composite from nano to macroscale. Nanotechnol Rev. 2021;10(1):636-52.
- Mittal G, Rhee KY, Mišković-Stanković V, Hui D. Reinforcements in multi-scale polymer composites: Processing, properties, and applications. Compos Part B Eng. 2018;138:122-39.
- [8] Lin H, Guo X, Song K, Feng J, Li S, Zhang X. Synergistic strengthening mechanism of copper matrix composite reinforced with nano-Al<sub>2</sub>O<sub>3</sub> particles and micro-SiC whiskers. Nanotechnol Rev. 2021:10(1):62-72.
- Han J, Wang D, Zhang P. Effect of nano and micro conductive materials on conductive properties of carbon fiber reinforced concrete. Nanotechnol Rev. 2020;9(1):445-54.
- [10] Ali A, Andriyana A. Properties of multifunctional composite materials based on nanomaterials: a review. RSC Adv. 2020;10(28):16390-403.
- De Cicco D, Asaee Z, Taheri F. Use of nanoparticles for [11] enhancing the interlaminar properties of fiber-reinforced composites and adhesively bonded joints - a review. Nanomaterials. 2017;7(11):360.
- [12] Kazemi-Khasragh E, Bahari-Sambran F, Siadati SMH, Eslami-Farsani R, Arbab, Chirani S. The effects of surface-modified graphene nanoplatelets on the sliding wear properties of basalt fibers-reinforced epoxy composites. J Appl Polym Sci. 2019;136(39):47986.
- Abdi A, Eslami-Farsani R, Khosravi H. Evaluating the mechan-[13] ical behavior of basalt fibers/epoxy composites containing surface-modified CaCO<sub>3</sub> nanoparticles. Fibers Polym. 2018;19(3):635-40.
- [14] Azizi H, Eslami-Farsani R. Study of mechanical properties of basalt fibers/epoxy composites containing silane-modified nanozirconia. J Ind Text. 2019;1528083719887530.
- [15] Lee W, Lee JU, Cha H-J, Byun J-H. Partially reduced graphene oxide as a multi-functional sizing agent for carbon fiber composites by electrophoretic deposition. RSC Adv. 2013:3(48):25609-13.
- [16] Agrawal M, Prabhakaran RTD. Effect of fiber sizing on mechanical properties of carbon reinforced composites: a review. Org Polym Mater Res. 2019;1(2). doi: 10.30564/ opmrv1i21683.2020.
- [17] Bergeret A. 3 Surface treatments in fiber-reinforced composites. In: Joseph K, Oksman K, George G, Wilson R, Appukuttan S, editors. Fiber reinforced composites. United Kingdom: Woodhead Publishing; 2021. p. 47-81.
- Kim S-H, Park S-M, Park S-J. Role of dry ozonization of basalt fibers on interfacial properties and fracture toughness of epoxy matrix composites. Nanotechnol Rev. 2021;10(1):710-8.
- [19] Dhand V, Mittal G, Rhee KY, Park S-J, Hui D. A short review on basalt fiber reinforced polymer composites. Compos Part B Eng. 2015;73:166-80.
- [20] Mittal G, Rhee KY. Chemical vapor deposition-based grafting of CNTs onto basalt fabric and their reinforcement in epoxybased composites. Compos Sci Technol. 2018;165:84-94.
- [21] Zhang Y, Mi C. Improved hydrothermal aging performance of glass fiber-reinforced polymer composites via silica nanoparticle coating. J Appl Polym Sci. 2020;137(19):48652.

- [22] Atiq Ur Rehman M, Chen Q, Braem A, Shaffer MSP, Boccaccini AR. Electrophoretic deposition of carbon nanotubes: recent progress and remaining challenges. Int Mater Rev. 2020;1–30.
- [23] Kim J, Cote LJ, Huang J. Two dimensional soft material: new faces of graphene oxide. Acc Chem Res. 2012;45(8):1356-64.
- [24] Lee XJ, Hiew BYZ, Lai KC, Lee LY, Gan S, Thangalazhy-Gopakumar S, et al. Review on graphene and its derivatives: synthesis methods and potential industrial implementation. J Taiwan Inst Chem Eng. 2019;98:163–80.
- [25] Chen J, Yao B, Li C, Shi G. An improved hummers method for eco-friendly synthesis of graphene oxide. Carbon. 2013:64:225–9.
- [26] de Moraes ACM, Lima BA, de Faria AF, Brocchi M, Alves OL. Graphene oxide-silver nanocomposite as a promising biocidal agent against methicillin-resistant Staphylococcus aureus. Int J Nanomed. 2015;10:6847-61.
- [27] Ma Y, Han J, Wang M, Chen X, Jia S. Electrophoretic deposition of graphene-based materials: a review of materials and their applications. J Mater. 2018;4(2):108-20.
- [28] Chua CK, Pumera M. The reduction of graphene oxide with hydrazine: elucidating its reductive capability based on a reaction-model approach. Chem Commun. 2016;52(1):72-5.
- [29] Deng C, Jiang J, Liu F, Fang L, Wang J, Li D, et al. Influence of graphene oxide coatings on carbon fiber by ultrasonically assisted electrophoretic deposition on its composite interfacial property. Surf Coat Technol. 2015;272:176–81.
- [30] Wu Y, Tang B, Liu K, Zeng X, Lu J, Zhang T, et al. Enhanced flexural properties of aramid fiber/epoxy composites by graphene oxide. Nanotechnol Rev. 2019;8(1):484–92.
- [31] Willemse CM, Tlhomelang K, Jahed N, Baker PG, Iwuoha EI. Metallo-graphene nanocomposite electrocatalytic platform for the determination of toxic metal ions. Sensors. 2011;11(4):3970-87.
- [32] Zakaria MR, Akil HM, Omar MF, Abdullah MMAB, Rahman AAA, Othman MBH. Improving flexural and dielectric properties of carbon fiber epoxy composite laminates reinforced with carbon nanotubes interlayer using electrospray deposition. Nanotechnol Rev. 2020;9(1):1170–82.

- [33] Nandi A, Das S, Halder S, Chakraborty A, Imam MA.

  Ultrasonically assisted electrophoretic deposition of oxidized graphite nanoparticle onto carbon fiber, amending interfacial property of CFRP. J Composite Mater. 2019;54(13):1615–25.
- [34] Kim D, Mittal G, Kim M, Kim S, Yop Rhee K. Surface modification of MMT and its effect on fatigue and fracture behavior of basalt/epoxy based composites in a seawater environment. Appl Surf Sci. 2019;473:55-8.
- [35] Hashim UR, Jumahat A, Jawaid M. Mechanical properties of hybrid graphene nanoplatelet-nanosilica filled unidirectional basalt fibre composites. Nanomaterials (Basel). 2021; 11(6):1468. doi: 10.3390/nano11061468.
- [36] Sumit Dash S, Gangineni PK, Gupta KBNVSG, Dasari S, Prusty RK, Ray BC. Evaluation of mechanical behavior of graphene oxide grafted CFRP composites: a comparison of anodic and cathodic EPD. Advances in materials and processing technologies; 2021. p. 1–9.
- [37] Berman D, Erdemir A, Sumant AV. Graphene: a new emerging lubricant. Mater Today. 2014;17(1):31–42.
- [38] Kumar S, Singh KK, Ramkumar J. The effects of graphene nanoplatelets on the tribological performance of glass fiber-reinforced epoxy composites. Proc Inst Mech Eng Part J J Eng Tribol. 2020;235(8):1514–25.
- [39] Wang D, Zhang D, Wang S, Ge S. Finite element analysis of hoisting rope and fretting wear evolution and fatigue life estimation of steel wires. Eng Fail Anal. 2013;27:173-93.
- [40] Baig MMA, Samad MA. Epoxy\epoxy composite\epoxy hybrid composite coatings for tribological applications a review. Polymers. 2021;13(2):179.
- [41] Wang B, Han W, Ming Y, Zhang X, Zhu Y, Duan Y, et al. Preparation and tribological study of graphene coating on glass fiber-reinforced composite using modified percolatingassisted resin film infusion method. Mater (Basel). 2020;13(4):851.
- [42] Vázquez-Moreno JM, Sánchez-Hidalgo R, Sanz-Horcajo E, Viña J, Verdejo R, López-Manchado MA. Preparation and mechanical properties of graphene/carbon fiber-reinforced hierarchical polymer composites. J Compos Sci. 2019;3(1):30.